Journal of Extracellular Vesicles

RESEARCH ARTICLE OPEN ACCESS

Intercellular Epigenomic Signalling via Extracellular Vesicles During B Cell Maturation

Kevin Ho Wai Yim[1,2] | Ala'a Al Hrout[1] | Richard Chahwan[1,2]

[1]Institute of Experimental Immunology, University of Zurich, Zurich, Switzerland | [2]EVIIVE AG, Zurich, Switzerland

Correspondence: Richard Chahwan (richard.chahwan@uzh.ch)

Received: 20 March 2024 | **Revised:** 18 December 2024 | **Accepted:** 5 January 2025

Funding: R.C. is supported by SNF (310030_212553; 320030E_215576, CRSK-3_190550; IZSEZ0_204655; IZSEZ0_218166), Novartis Foundation (22B140), Vontobel Stiftung (41309), UZH-STWF (F-41309-01-01) and the UZH-URPP (Translational Cancer Research). K.Y. is supported by a BioMedTech Entrepreneur Fellowship, BRIDGE-SNF (40B1-0_221565) and GRS-Innobooster (GRS-069/23). Funding for open access charge: SNSF-Chronoshub.

Keywords: antibody maturation | extracellular vesicles | intercellular epigenomic signalling | non-coding RNA | single particle analysis

ABSTRACT

B cell maturation is crucial for effective adaptive immunity. It requires a complex signalling network to mediate antibody diversification through mutagenesis. B cells also rely on queues from other cells within the germinal centre. Recently, a novel class of intercellular signals mediated by extracellular vesicles (EVs) has emerged. Studies have shown that B cell EV-mediated signalling is involved in immune response regulation and tumorigenesis. However, the mechanistic role of B cell EVs is not yet established. We herein study the biological properties and physiological function of B cell EVs during B cell maturation. We use emerging technologies to profile B cell EV surface marker signatures at the single particle level, molecular cargo and physiological roles in B cell maturation. EV ncRNA cargo, characterised by RNA-seq, identified an EV-mediated novel non-coding RNA (ncRNA) regulatory network for B cell maturation. We show that a previously uncharacterised micro-RNA (miR-5099) in combination with a set of long ncRNA are carried within B cell EVs and could contribute to antibody diversification. The physiological role of EVs in B cell maturation is investigated using EV blockade assays and complementation studies using diverse EV sources further confirmed the physiological role and mode of action of EVs in B cell maturation.

1 | Introduction

Adaptive immunity is one of the main strategies used by vertebrates to protect against infections. In particular, research on B cells - the producers of high-affinity antibodies to mediate specialised immune responses - has garnered significant attention (Bonilla and Oettgen 2010). The key processes involved in B cell antibody diversification and affinity maturation are known as class switch recombination (CSR) and somatic hypermutation (Muramatsu et al. 2000; Morrish et al. 2019; Wang et al. 2022). CSR is a B cell-specific intrachromosomal rearrangement of the switch region of the immunoglobulin (Ig) locus, from IgM to different isotypes, which results in the generation of repertoire of antibodies (i.e., IgG1, IgG3, IgA, IgE) with different effector functions against invading pathogens. Defects in CSR in humans lead to immunodeficiency phenotypes such as hyper-IgM syndrome (Jhamnani et al. 2018). The mechanism of CSR is a rather complex process that is orchestrated by a number of molecules and signalling factors. Murine primary splenic B cells have been widely used to study CSR regulation ex vivo with maximum CSR to IgG1 to around 20%, until the establishment of CH12F3, a high CSR efficiency (up to 60% CSR to IgA) cell line developed in 1996 (Muramatsu et al. 2000). However, the rationale for such significant difference in CSR efficiency between the two cell types

is unclear. In addition, endogenous expression of CSR and DNA damage repair (DDR) associated genes between the two cell types cannot account for such differences.

Studies have shown that non-coding RNAs (ncRNAs) are able to modulate B cell development and CSR (Sheppard et al. 2018; Ho et al. 2022; Yim et al. 2023). Small ncRNAs like miR-181b and miR-361 can silence AID expression in B cells and reduce CSR efficiency. Depletion of miR-155 in activated B cells reduces the production of IgG1+ plasma cells and memory B cells and therefore loss of IgG1+ antibodies (Vigorito et al. 2007). Extracellular vesicles (EVs), a new class of intercellular communication players, have been shown to deliver RNA and proteins, especially ncRNAs, from one cell and another to modulate gene expression in recipient cells (Yim et al. 2020). Although recent studies have shown EVs released by B cells can trigger primed $CD4^+$ T cells proliferation and T_H2-like cytokine production via delivery of MHC complexes (Muntasell, Berger and Roche 2007; Admyre et al. 2007), inter B cell communication via EVs in physiological conditions requires further investigation. In this study, we attempted to understand the biological properties of B cell EVs during CSR that might contribute to physiological B cell development, and more importantly to determine whether the unknown difference in CSR efficiency between primary B cells and CH12F3 could be explained via EV-mediated signalling. Our findings demonstrate, for the first time, significant increase of CSR in primary B cells via culturing in fresh CH12F3-derived conditioned media, but not in freeze-thawed media. The latter condition acts as an EV control since intact EVs are ruptured by freeze-thaw cycles whilst other cell-free proteins, nucleic acids and cytokine factors should be retained. Strikingly, the vice versa combination led to drastic reduction of CSR in CH12F3, suggesting the existence of EV-mediated CSR regulation in B cells. Differential expression (DE) of surface markers and EV ncRNA cargo during CSR was revealed with a specialised nanoparticle flow cytometer (NanoFCM) and ncRNA-seq. Moreover, our data suggested effective EV-mediated CSR regulation requires the presence of EV surface proteins and molecular cargo. Mechanistically, we identified a novel CSR suppressor, miR-5099, an uncharacterised miRNA that was only upregulated in stimulated B cell EVs, but not CH12F3 EVs. We also identified a long ncRNA CSR activator, Gm26917 that was upregulated in stimulated CH12F3 EVs. Taken together, these findings not only decipher the intrinsic difference in CSR efficiency between primary B cells and CH12F3 but also provide a novel perspective to study T cell-independent CSR regulation via EVs.

2 | Materials and Methods

2.1 | Cell Cultures and In Vitro/Ex Vivo CSR

CH12F3 cells were maintained and CSR assays performed as described previously (Nakamura et al. 1996). In brief, cells were stimulated with 1 ng/mL of recombinant human TGF-β1 (R&D Systems), 10 ng/mL of recombinant mouse IL-4 (R&D Systems) and 2 μg/mL of functional-grade purified anti-mouse CD40 (eBiosciences) and then analysed by flow cytometry as described below. Splenic B cells were obtained from WT 8-week-old female mice. Purified B cells were plated at a concentration of 0.5×10^6 cells/mL and stimulated with either 50 μg/mL LPS (Sigma-Aldrich) or 50 μg/mL LPS and 50 ng/mL rIL-4 (R&D Systems) for 4 days. Animal protocols were reviewed and approved by the veterinary office of the canton of Zurich, Switzerland (213/2020).

2.2 | Isolation of EVs From Cell Cultures

Splenic B cells and CH12F3 were cultured for 2 days in RPMI 1640 plus particulate-depleted 10% FCS. FCS EVs were depleted using an ultrafiltration filter (Amicon Ultra-15 100 kDA) at 3000 × *g* for 55 min. Culture supernatants were first spun at 400 × *g* for 5 min to deplete cells and then at 10,000 × *g* for 20 min to deplete residual cellular debris. EVs were isolated by 100,000 × *g* ultracentrifugation for 2 h at 4°C, and finally resuspended in PBS for further nanoflow analysis and functional assays. To deplete surface proteins on EVs surface, purified EVs in PBS were treated with Proteinase K (Thermo Fisher, 50 ng/μL) for 30 min at 37°C then quenched by incubation at 75°C for 5 min. To deplete EVs in suspension, purified EVs in PBS were ruptured by at least three cycles of freeze-thaw or incubated with 1% Triton-X for 15 min at room temperature.

2.3 | Transmission Electron Microscopy (TEM) of Purified EVs

To visualise EV samples under the transmission electron microscope samples were transferred onto pioloform-coated EM copper grids by floating the grids on a droplet containing freshly prepared exosome placed on parafilm. After 5 min of incubation, the grids were washed 3 × 5 min on droplets of deionised water before contrasting of bound exosomes in a mixture of 2% w/v methyl cellulose and 2% w/v uranyl acetate (mix 9:1) on ice for 10 min. Contrasted grids were then air-dried in a wire loop before analysis using a JEOL JEM 1400 transmission electron microscope operated at 120 kV. Images were taken with a digital camera (ES1000W, Gatan, Abingdon, UK). For immunogold labelling, exosomes were transferred onto EM grids as described above. After 3 × 5 min washes in deionised water unspecific binding sites were blocked with 0.5% fish skin gelatin (FSG) in PBS for 10 min before incubation with gold conjugated mouse IgM antibody (G5652, Sigma Aldrich) for 30 min. After 3 × 5 min washes in PBS, the grids were incubated with 10 nm protein A gold (BBI Solutions, Cardiff, UK) for 20 min before washing the grids again in PBS (6 × 5 min) followed by 10 × 1 min washes in deionised water. Exosomes were then contrasted and imaged as described above.

2.4 | Immunoblotting

Purified EVs were lysed with RIPA buffer and heated at 95°C for 10 min before loading 50 μg of total protein for electrophoresis. The membrane was incubated with a primary rabbit anti-CD63 antibody (10628D, Invitrogen), anti-Alix (Ma1-83977, Invitrogen), anti-CD19 (14-0194-82, Invitrogen), anti-AID (14-5959-80, Invitrogen) and anti-Golgin 97 (PA5-30048, Invitrogen) overnight at 4°C on a shaker. Membranes were washed with TBST three times at 15-min intervals. The goat anti-rabbit IRDye 680 RD secondary antibody (1:1000 dilution, Li-COR, catalogue number: 925–68071) was then incubated with the membrane for 1 h at

room temperature. Blots were imaged using the Li-COR Odyssey scanner after washing.

2.5 | Immunostaining and Flow Analysis of Cells

Surface IgM, IgA, IgG1 on CH12F3 and primary B cells were determined by BD FACSCanto II cell analyser with APC-eFluor 780 anti-mouse IgM (47-5790-82 eBioscience), FITC anti-mouse IgA (11-4204-81, eBioscience) and PE anti-mouse IgG1 (12-4015-82, eBioscience) antibodies. Cells were washed in PBS at 300 × *g* for 5 min. Antibody staining was performed at a concentration of 1 in 200. Stained cells were washed once with PBS before acquisition. Gating was based on single cells followed by cell viability staining (65-0866-14, Thermo Fisher). All data analysis of cells and EVs were carried out with FlowJo (TreeStar) software and Graphpad Prism 9 software.

2.6 | Immunostaining and Nanoflow Analysis of Purified EVs

Purified EVs were stained with FITC anti-mouse IgA (11-4204-81, eBioscience), FITC anti-mouse IgG1 (11-4015-82, eBioscience), PE anti-mouse IgM (12-5790-82, eBioscience), FITC Rat IgG2b, κ Isotype Ctrl (400633, Biolegend), FITC anti-mouse CD9 (124807, Biolegend), FITC anti-mouse CD19 (302206, Biolegend) and followed by 100,000 × *g* for 2 h at 4°C to remove unbound antibodies. Stained EVs were resuspended in 100 μL of 0.22 μm filtered PBS and subjected to flow analysis by NanoFCM Flow Nanoanalyzer. Monodisperse silica nanoparticles of four assorted sizes, with modal peak sizes of 66, 91, 113 and 155 nm were used as the size reference standard to calibrate the size distribution of EVs. Unless stated otherwise, all samples were recorded in 1 min with the range of 2000–12,000 events per minute to minimise the swarm detection effect since there is enough time/space between each particle measurement as evinced by the event burst trace which shows separate measurements of particles. The steady flow of the system allows for comparison of particle detection rate to a concentration standard (a stable 250 nm silica bead of 1.87e10/mL [batch variable]). The particle concentration is then calculated, including the dilution factor, in particles/mL. All data analysis of cells and EVs were carried out with FlowJo (TreeStar) software and Graphpad Prism 9 software.

2.7 | RNA Extraction

Cell and EV total RNA were extracted by Trizol (Invitrogen) and purified by RNeasy Mini Kit (Qiagen). Briefly, cell or EV pellets 700 μL Trizol. Subsequently, 140 μL of chloroform was used for phase separation. Trizol and chloroform mix were centrifuged at 12,000 × *g* for 15 min for phase separation. 300 μL RNA-containing top clear phase was transferred to a fresh tube and 400 μL absolute ethanol was added and mixed. 700 μL of sample were transferred to RNeasy spin column. DNAse treatment was performed after the first 350 μL RW1 washing step. Finally, RNA was eluted in 30 μL RNase-free water. RNA concentration was assessed using a NanoDrop 2000 spectrophotometer (Thermo Scientific, Waltham, MA, USA). The RNA yield and size distribution were analysed using an Agilent 2200 Tapestation with high-sensitivity RNA Screentape (Agilent Technologies, Foster City, CA, USA).

2.8 | RNA-Seq Library Preparation, Next-Generation Sequencing and Data Processing

For small RNA library preparation, RNA aliquots were used for library preparation using NEBNext Multiplex Small RNA library preparation kit (New England Biolabs, Ipswich, MA, USA). The PCR-amplified cDNA construct (from 140 to 160 bp) was purified using a QIAquick PCR Purification kit (Qiagen). The purified cDNA was directly sequenced using an Illumina MiSeq 2000 platform (Illumina, San Diego, CA, USA).

For long ncRNA library preparation, libraries were constructed using Ribo-Zero Magnetic Gold Kit (Human) (Illumina, San Diego, CA, USA) and NEBNext Ultra RNA Library Prep Kit for Illumina (New England Biolabs) according to the manufacturer's instructions. Libraries were tested for quality and quantified using qPCR (Kapa Biosystems, Woburn, MA, USA). The resulting libraries were sequenced on a HiSeq 2500 instrument that was generated with either single-end (CH12F3) or paired-end (primary B cells) reads of 100 nucleotides.

Raw sequencing reads were checked for potential sequencing issues and contaminants using FastQC. The RNA-seq data has been deposited in the Gene Expression Omnibus (GEO) database with the accession number GSE242731. Adapter sequences, primers, number of fuzzy bases (Ns) and reads with quality scores below 30 were trimmed using fastq-mcf. Clean reads were aligned to the mouse genome (GRCm38/mm10.p6; September 2019) using the TopHat 2.0 program, and the resulting alignment files were reconstructed with Cufflinks (Trapnell et al. 2014). The transcriptome of each sample was assembled separately using the Cufflinks 2.0 program. All transcriptomes were pooled and merged to generate a final transcriptome using Cuffmerge. After the final transcriptome was produced, Cuffdiff was used to estimate the abundance of all transcripts based on the final transcriptome to generate read counts for each sample.

2.9 | Gene Expression Quantification by RT-qPCR

Altogether 800 ng total RNA was converted into cDNA using a High-Capacity cDNA Reverse Transcription Kit according to manufacturer's protocol. qPCR was performed using HOT FIREPol EvaGreen qPCR Mix Plus no ROX (Solis Biodyne) and analysed with a Bio-Rad CFX384 Touch Real-Time PCR Detection System. Oligo names and sequences are provided in Table S2.

2.10 | Sequencing Data Analyses and Statistical Methods

Read counts of each sample were subjected to cluster analysis and DE analysis using the standard DESeq2 package on RNA-seq 2G online platform (Zhang et al. 2017). |fold-change| ≥1, p value ≤ 0.05 and false discovery rate (FDR) ≤0.05 was considered statistically significant DE ncRNAs. DE ncRNAs expression in different immune cell types was determined using My Geneset

from the ImmGen database (Heng et al. 2008). Interaction and gene targets of identified DE ncRNAs in cells and paired EVs were predicted by miRNet and ENCORI (Fan et al. 2016; Li et al. 2014). Motif analysis were performed using XSTREME motif discovery and enrichment analysis software (Bailey et al. 2015). Briefly, FASTA sequence of miRNAs in each sample (e.g., cells vs. paired EVs; unswitched EVs vs. switched EVs) were used as input for RNA motifs discovery and enrichment analysis (Ray2013 All Species), Analytical parameters were set as following, E value ≤ 10, motif width between 4 and 15 and alignment starting from left ends. Motifs with over 50% true-positive and 0% false-positive enrichment were selected as unique motifs for indicated sample.

2.11 | EV Blockade and Gene Silencing/Overexpression Assay

10 and 5 μM GW4869 was used to block EV production in CH12F3 and primary B cells respectively prior to cytokine activation. Expression of target ncRNAs in CH12F3 and primary B cells were inhibited by 2 μM miRCURY LNA miRNA Inhibitors (339131, Qiagen), anti-miR-5099 (GGAGCACCACATCGATCTAA-FAM); antimir-control (TAACACGTCTATACGCCCA-FAM), Antisense LNA GapmeR for Gm26917 was designed using the LNA GapmeR designer (Qiagen). Transfection efficiency was quantified by FAM signal intensity increase prior to cytokine activation. Overexpression of miR-5099 in CH12F3 was achieved by transfecting 2 μM of miR-5099 miRCURY LNA miRNA mimic (Qiagen) by electroporation using Lonza 4D-Nucleofector and cell line SF kit following manufacturer's protocol.

2.12 | EV Uptake Assay

For EV uptake assay, CH12 cells were divided into two tubes for staining to distinguish the exchange of EVs between the two populations. Cells were counted to have 1 × 105/well and stained with either CellTrace Yellow (C34567, Invitrogen) or CSFE (423801, Biolegend), at a final concentration of 1uM. Cells were incubated at 37°C for 20 min in the dark. Excess dye was quenched with complete culture media. Cells were resuspended in 1 mL complete culture media in 24-well plates and allowed to rest for 24 h prior to co-culture for an additional 24 h. Samples were analysed with FACS to analyse CFSE uptake in cell trace stained cells. Briefly, all cells were washed and collected by centrifugation at 300 × g for 5 min and washed with PBS. Samples were acquired using Cytek Aurora 5L.

2.13 | Data and Statistical Analysis

Flow cytometry data was exported as FCS files and analysed using Flowjo software (Treestar). NanoFCM propriety software was used to generate FCS files and analytical reports with information regarding the sample concentration and mean particle size for all EV samples. Statistical analysis of flow cytometry values, qPCR data and RNA-seq data were performed using GraphPad (version 9.1.1, GraphPad Software, La Jolla California, USA) using one-way or two-way ANOVA with Tukey's multiple comparison test, where $^{*}p < 0.05$, $^{**}p < 0.01$, $^{***}p < 0.001$.

3 | Results

3.1 | Extracellular Constituents Are Required for High CSR Efficiency in B Cells

Primary splenic B cells has been the classical study model for CSR, until the emergence of CH12F3, a high switching frequency and single isotype committed (IgA exclusively) cell line established by Honjo et al. (Muramatsu et al. 2000). We compared the CSR efficiency of primary B cells (from IgM^+ to $IgG1^+$) and CH12F3 (from IgM^+ to IgA^+), upon cytokine stimulation, in both our own assays as well as results from other publications (Liu et al. 2017; Lee-Theilen et al. 2011; Thomas-Claudepierre et al. 2013; Xu et al. 2012; Chahwan et al. 2012; Ramachandran et al. 2010) (Figure 1A). A significant difference in switching efficiency was observed, with ∼20% switching in primary B cells and ∼60% switching in CH12F3. However, the intracellular molecules responsible for such differences has not been identified so far, despite several multi-omics studies. Therefore, we explored the possibilities of extracellular mediated CSR regulation by culturing primary B cells in conditioned medium (CM) from stimulated CH12F3, and vice versa (Figure 1B). CM from both cell types were either used directly or after three freeze thawing cycles to retain only potential functional cytokines, proteins and nucleic acids, but not intact EVs (Figure S1) (Hale et al. 2021; Simpson et al. 2020; Ji et al. 2017; Liu et al. 2021; Wang et al. 2015). Strikingly, significant increase in primary B cells CSR to $IgG1^+$ was observed in CH12F3 CM condition, but not in freeze thawed CM, compared to autologous CM control (Figure 1C). Moreover, CH12F3 switching to IgA+ was drastically reduced only when cultured in fresh primary B cell CM, compared to the autologous CM control (Figure 1D). The loss of function in freeze-thawed CM underscores the significant contribution of EVs. Neither the free-floating proteins nor the nucleic acids retained in the freeze-thawed CM were able to produce comparable regulatory effects.

EV transfer and uptake were further confirmed by the culture of CH12F3 cells independently labelled with CFSE (green; Figure S1A) and CellTrace (orange; Figure S1A). The expectation from such setting is that cells that have acquired double staining, in a co-culture setup, are likely the result of active EV transfer between cells since both CFSE and CellTrace are inactivated by cell culture media. We observed that double positive staining signals only increased in the co-cultured condition but not in the CFSE or CellTrace mono-cultures. This supports the notion that $CFSE^+$ CH12F3 EVs were successfully uptaken by CellTrace-labelled recipient CH12F3 cells (Figure S2) These findings support the existence of EV-mediated intercellular signalling during B cell maturation, independent of T cell-mediated signalling.

3.2 | CSR Causes Differential Surface Proteins and Cargo Profiles on Released EVs

To better understand how CSR affects the biological properties of B cell EVs, we analysed EVs from B cells with or without cytokine stimulation. Since culturing primary B cells ex vivo requires stimulation for survival after purification from spleens, thus, it was not possible to isolate EVs from unstimulated primary B cells per se. For this matter, we used CH12F3 EVs as our

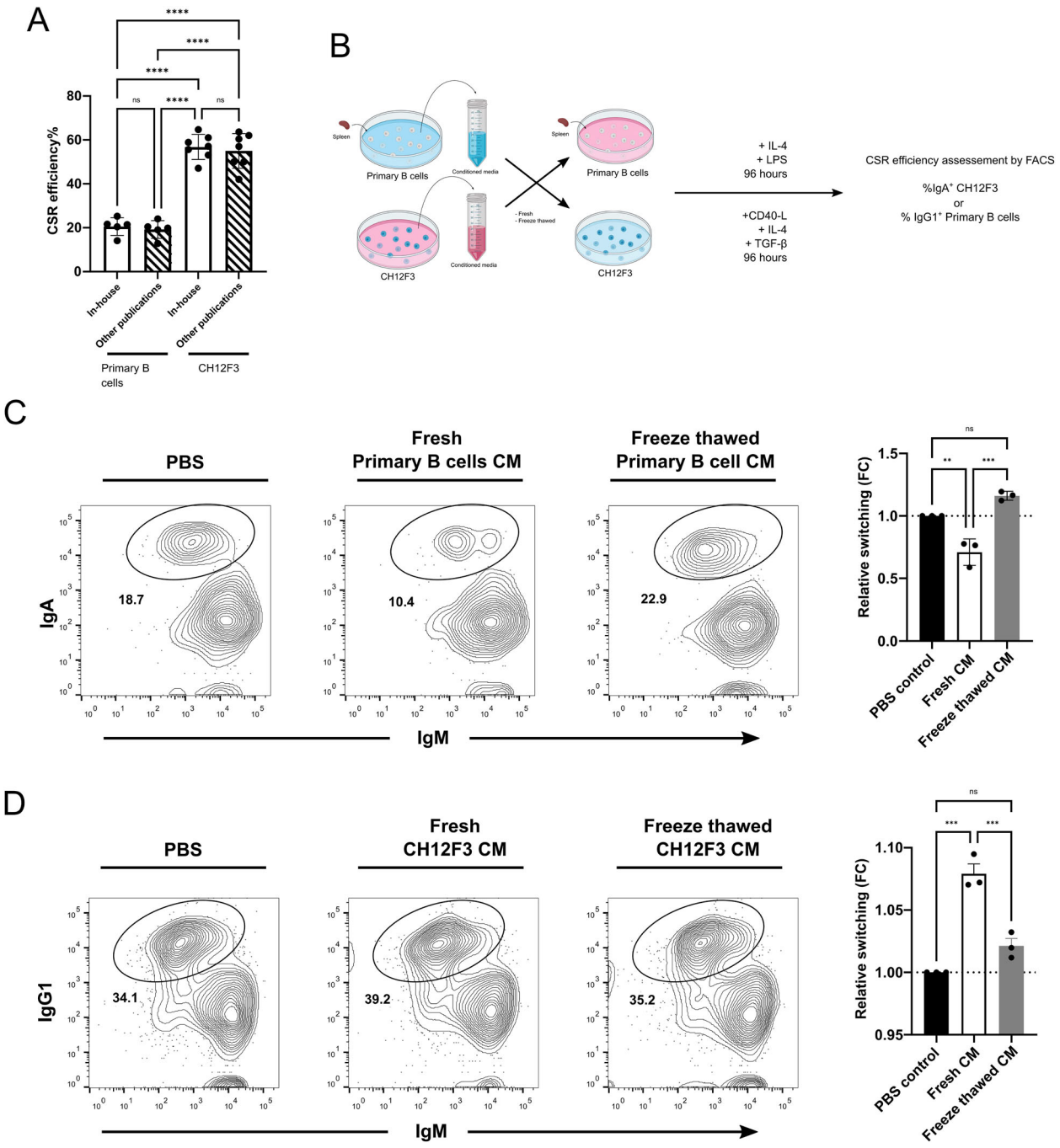

FIGURE 1 | Extracellular constituents from different B cell lines regulate CSR. (A) Comparison of CSR efficiency in primary splenic B cells and CH12F3 from own data and other published data. (B) Schematic outline of conditioned medium exchange experiment. (C and D) Representative FACS plots and quantifications of CSR efficiency of IgG1 CSR of primary splenic B cells (C) and IgA CSR of CH12F3 (D) in the presence of denoted conditions. Representative of three experiments, mean ± SD shown in columns by one-way ANOVA with Tukey's multiple comparison test (*$p < 0.05$; **$p < 0.01$; ***$p < 0.001$).

study model here since they undergo CSR with higher efficiency compared to other cell lines, and more vitally, the possibility to isolate EVs from unstimulated state. EVs from unstimulated and stimulated CH12F3 were prepared as described (Figure 2A). In addition, foetal calf serum a main ingredient in mammalian cell culture media contained a significant amount of heterologous EVs (bovine EVs) that may also affect B cell survival and isotype switching efficiency (Figure S3). Western Blot analysis of CH12F3 and released EVs with or without stimulation showed a differential protein expression profile. Interestingly, we observed that the pan-B cell marker, CD19 was as highly expressed in EVs as the parental cells, suggesting the potential usage of EVs as a B cell-specific biomarker. The classical EV tetraspanins marker, CD63 was not highly expressed in CH12F3 EVs which correspond to other publications (Saunderson et al. 2008). One of the most vital mediators for CSR, AID protein, was not or lowly detectable in stimulated CH12F3 EVs, suggesting the CSR regulatory function by EV signalling was not mediated by direct delivery of AID

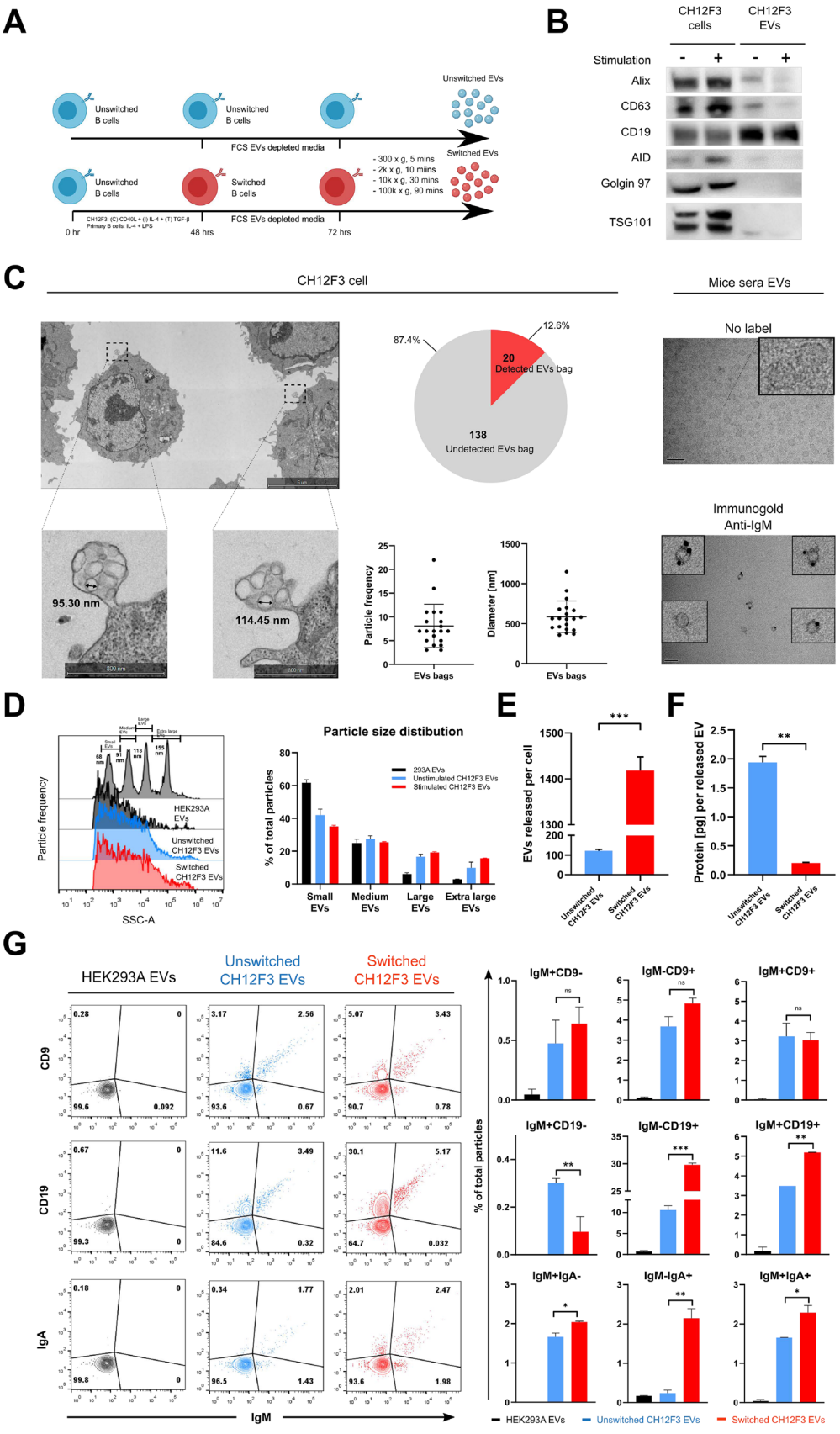

FIGURE 2 | Multiplex characterisation of B cell EVs during CSR. (A) Schematic outline of cell stimulation and EV collection. (B) Western blot analysis of denoted protein markers from CH12F3 and derived EVs during CSR. (C) Left: transmission electron microscopy analysis of CH12F3, with suspected EV bags morphology and quantification. Right: Immuno-gold labelling of IgM in mice serum EVs. (D) Representative side scatter plot and estimated size distribution quantification of CH12F3 EVs during CSR, using silica sizing beads with mix of 66 nm (small), 91 nm (medium), 113 nm

(large), and 155 nm (extra-large) (r index = 1.46). (E) Quantification of estimated EV particles released per cell via dividing the total number of particles by number of parental cells. (F) Quantification of estimated EV proteins per released particle via dividing the total amount of EV proteins by number of particles. (G) Representative FACS plots and quantification of denoted markers of CH12F3 EVs during CSR. Antibodies used are anti-mouse to target murine CH12F3 B with human epithelial HEK293 cells acting as a staining control. Representative of three experiments, mean ±SD shown in columns by one-way ANOVA with Tukey's multiple comparison test (*$p < 0.05$; **$p < 0.01$; ***$p < 0.001$).

(Figure 2B). TEM analysis in our data revealed pockets of exosome-sized vesicles being secreted by B cells. Using the MAPS software (Thermo Scientific) to perform high-resolution analysis, the sizes and quantification of individual vesicles as well as the entire pockets were determined. Strikingly, in one TEM cross-section (70 nm), vesicles pockets were found in 20 out of 158 cells which we estimated around 10 pockets being secreted by an actual B cell (between 7 and 10 μm) at any time point. Furthermore, the presence of B cell-derived EVs was readily detected in mice serum using anti-mouse IgM immunogold labelling, suggesting their biological relevance in physiological conditions (Figure 2C).

Next, single nanoparticle flow analyser, NanoFCM was used to profile surface markers, as well as sizes and quantity of CH12F3 EVs with or without stimulation. Using known size silica beads (r index: 1.46) as reference, the mean estimated sizes of unstimulated and stimulated CH12F3 EVs were ranging between 80 and 90 nm, which was comparable to our TEM data (Figures 2D and S4). The ratio between number of CH12F3 and their EVs were quantified, align with previous studies (Muntasell, Berger and Roche 2007; Saunderson et al. 2008), stimulated CH12F3 released 10-fold more EVs compared to unstimulated CH12F3, suggesting a correlation between cellular stress and EV secretion in B cells (Figure 2E). Interestingly, ratio between total protein and number of EVs in stimulated CH12F3 EVs was around 10-fold less compared to unstimulated CH12F3 EVs, indicating activated B cells selectively shuttle only the critical functional protein cargo into secreted EVs in exchange of higher EV secretion. (Figure 2F). Surface marker profile of EVs derived from CH12F3 with or without stimulation was determined, human embryonic kidney 293A (HEK293A) EVs were used as negative staining control. Potential fluorophores spillovers (co-labelling of FITC and PE conjugated antibodies) were also assessed using single stained EVs (Figure S5). Interestingly, only 10% of CH12F3 EVs express classical tetraspanins marker, CD9 and half of which also express IgM. CD9 expression on EVs was not significantly altered during CSR. The low expression of CD9 in the total CH12F3 EV population suggested that tetraspanins might not always be a generic marker of EVs purification or capture for FACS, especially for B cell EVs, and therefore, a more expressed marker will be needed for B cell EV studies. Pan-B cell marker, CD19 were expressed on 35% of total EV population from stimulated CH12F3, with 30% only $CD19^+$ and 5% IgM^+CD19^+. Here, we observed a 3-fold significant increase in CD19 expression on EVs during CSR, moreover, such increment was not detectable by Western Blot analysis. Surface IgM and IgA on EVs were compared during CSR. Amount of IgM^+ EVs were consistent during CSR, however, IgA^+ EVs were 5-fold more in CH12F3 after stimulation (Figure 2G). Similar results were also observed between unswitched (24 h post stimulation) and switched (72 h post stimulation) primary B cells derived EVs, including significant increased total EV secretion, elevated expression of CD9, CD19 and CSR specific IgG1 on secreted EVs during CSR (Figure S6) Taken together, these findings provided a novel comprehensive foundation for the field to better understand physiological EV-mediated signalling in B cells development.

3.3 | Differential EV ncRNAs Repertoire in Primary B and CH12F3 EVs

Increasing number of evidence has demonstrated different cell types actively and selectively shuttle ncRNAs cargo into secreted EVs to perform intercellular signalling in recipient cells (Yim et al. 2020). To explore the possibility of EV ncRNAs mediated regulation in B cell CSR, we performed RNA-seq analysis. Total RNA from the cells and EVs were extracted from unswitched and switched primary B cells and CH12F3 for exploratory screening (Figure 3A). Small RNA (< 200 nt) and lncRNA (> 200 nt) libraries were first prepared from extracted total RNA and subjected to RNA-seq analysis. The abundance of miRNAs and lncRNAs in CH12F3 and primary B cell-derived EVs with over 20 reads were quantified. LncRNAs were more represented in CH12F3 EVs compared to miRNAs in unswitched state (243 lncRNAs vs. 51 miRNAs), and further enriched after stimulation of parental cells (525 lncRNAs vs. 55 miRNAs). However, in primary B cell EVs, number of miRNAs and lncRNAs were similar in the unswitched state (45 lncRNAs vs. 49 miRNAs), and miRNAs were more enriched after switching (36 lncRNAs vs. 106 miRNAs) (Figure 3B, Supporting Files 1 and 2). Apart from ncRNAs abundance, ncRNAs expression between primary B cell and CH12F3 EVs was also significantly different as shown in the $\log_2$ transformed heatmap (Figure 3C), suggesting the two cell types have a vastly different EV cargo packaging regimen and thereby exert differential effect in CSR regulation. Other RNA biotypes, below and above 200 nt, were also quantified in primary B cells, CH12F3 and secreted EVs (Figure 3D). Differentially expressed mRNA during CSR in both primary B cells and CH12F3 and paired EVs were visualised, more overlapping mRNAs between parental cells and secreted EVs were observed in CH12F3 but not primary B cells (Figure S7).

To understand if B cells also selectively package miRNAs into secreted EVs as reported in a recent study (Garcia-Martin et al. 2022), differentially expressed miRNAs in paired cells and EVs, pre- and post-CSR from both CH12F3 and primary B cells were subjected to Simple Enrichment Analysis (Bailey et al. 2015) to identify motif enrichment in EVs compared to parental cells (Figure S8). Unique motifs enriched in cells or paired EVs were first selected and those expressed in at least 50% of input miRNAs and p value < 0.001 were then included in the list of motif candidates. Finally, for cells or EV enriched motifs, only the ones that were present in both primary B cells and CH12F3 throughout CSR were considered as potential conserved cell retaining and EV sorting motifs in B cells. In cell miRNA motifs, polyA sequence motifs were highly overrepresented throughout CSR in both

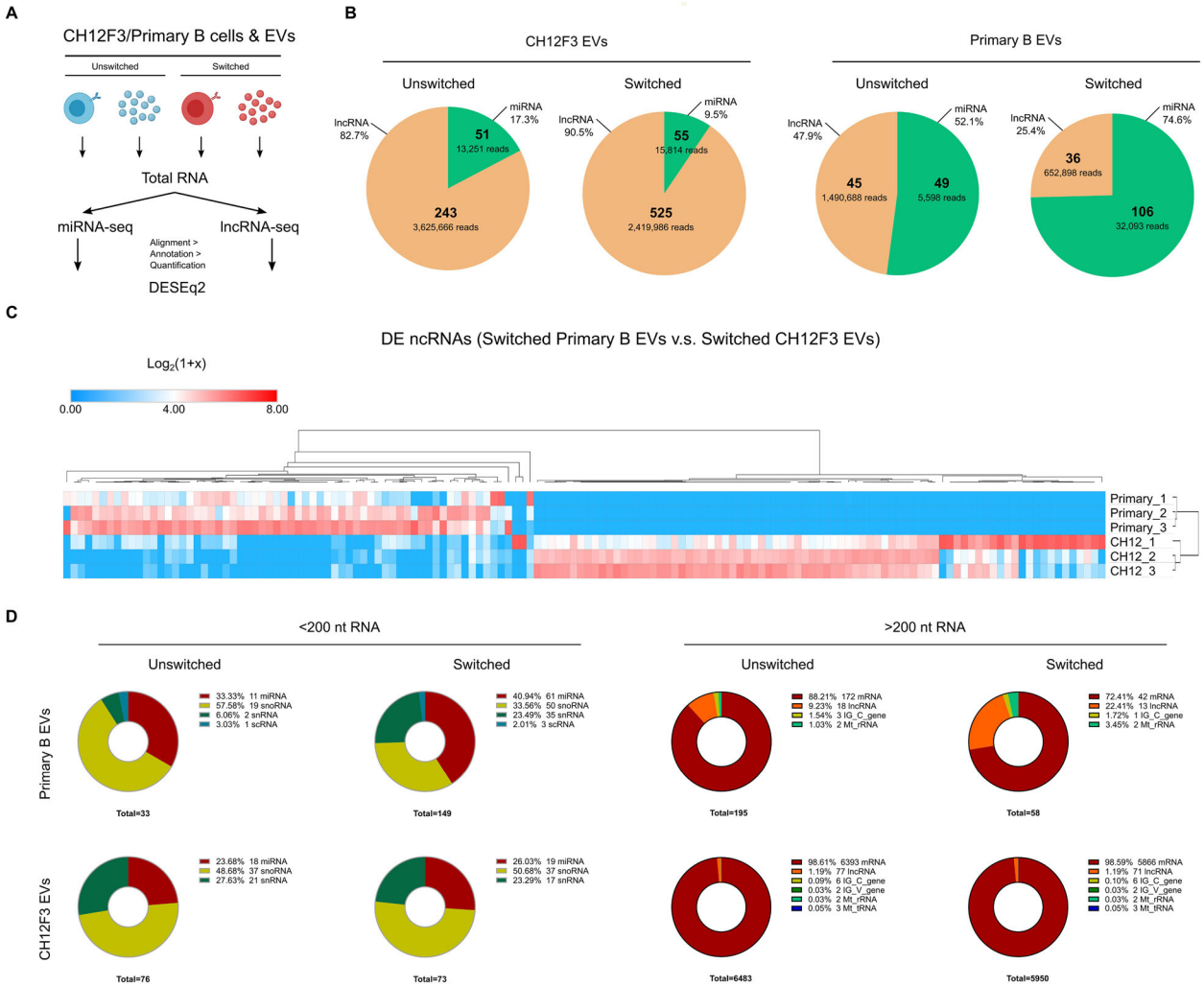

FIGURE 3 | Varied non-coding RNA profile in primary B cells EVs and CH12F3 EVs during CSR. (A) Schematic outline of RNA-seq analysis of molecular cargo in EVs and paired cells. (B) Quantification of non-coding RNA (ncRNA) reads (> 30 reads) from EVs in denoted conditions. (C) Expression heatmap of differentially expressed ncRNAs between primary B EVs and CH12F3 EVs. Hierarchical clustering by one minus spearman rank correlation of log2(1 + x) transformed read counts. (D) Quantification of other RNA biotypes, below and above 200 nucleotides, in primary B cells, CH12F3, and their secreted EVs during CSR.

primary B cells and CH12F3 and even more significant 4 days post CSR. Interestingly, three unique EV enriched motif consensuses, NACCYAA, VUWUCCC and AGAGAAA were identified throughout CSR in both EV sources, suggesting the existence of sequence motif-based miRNAs sorting mechanism in B cells (Figure S8).

3.4 | EV Mediated CSR Regulation Is Surface and Cargo Dependent

To determine the mode of EV-mediated CSR regulation, EV production in CH12F3 and primary B cells was first inhibited by GW4869 (Kosaka et al. 2010; Essandoh et al. 2015; Hu et al. 2019), a ceramide synthesis inhibitor prior to cytokine stimulation for CSR. The effect of GW4869 in suppressing EV production was assessed by comparing number of EV particles collected 24 h after treating with GW4869 with DMSO as control (Figure S9). At the same time, to validate the contribution of EVs in such regulation, but not other exogenous factors (i.e. proteins or cytokines), complement of autologous EVs in four forms, fresh, proteinase-K treated (depletion of protein aggregates and EV surface proteins) (Chettimada et al. 2018), triton-X-treated and freeze-thawed (depletion of intact EVs) (Figure 4A) was performed. As expected, the depletion of released EVs in CH12F3 resulted in reduction in CSR to IgA, however, CSR to IgG1 in primary B cells was enhanced compared to DMSO control. It further proved the existence of differential regulation mediated by EVs from the two cell types. Furthermore, complement of fresh autologous EVs was able to rescue the phenotype observed above, however, proteinase-K-treated EVs only showed half rescue compared to fresh EVs, and triton-X-treated EVs were not able to rescue the CSR reduction. Taken together, CH12F3 EVs are promoting CSR whilst primary B cell EVs are suppressive for CSR, and such EV-mediated CSR regulation is likely to be a dual-step process that relies on EVs surface proteins, possibly for docking and signal triggering, as well as molecular cargo delivered by intact EVs for gene modulation in recipient cells (Figure 4B, C).

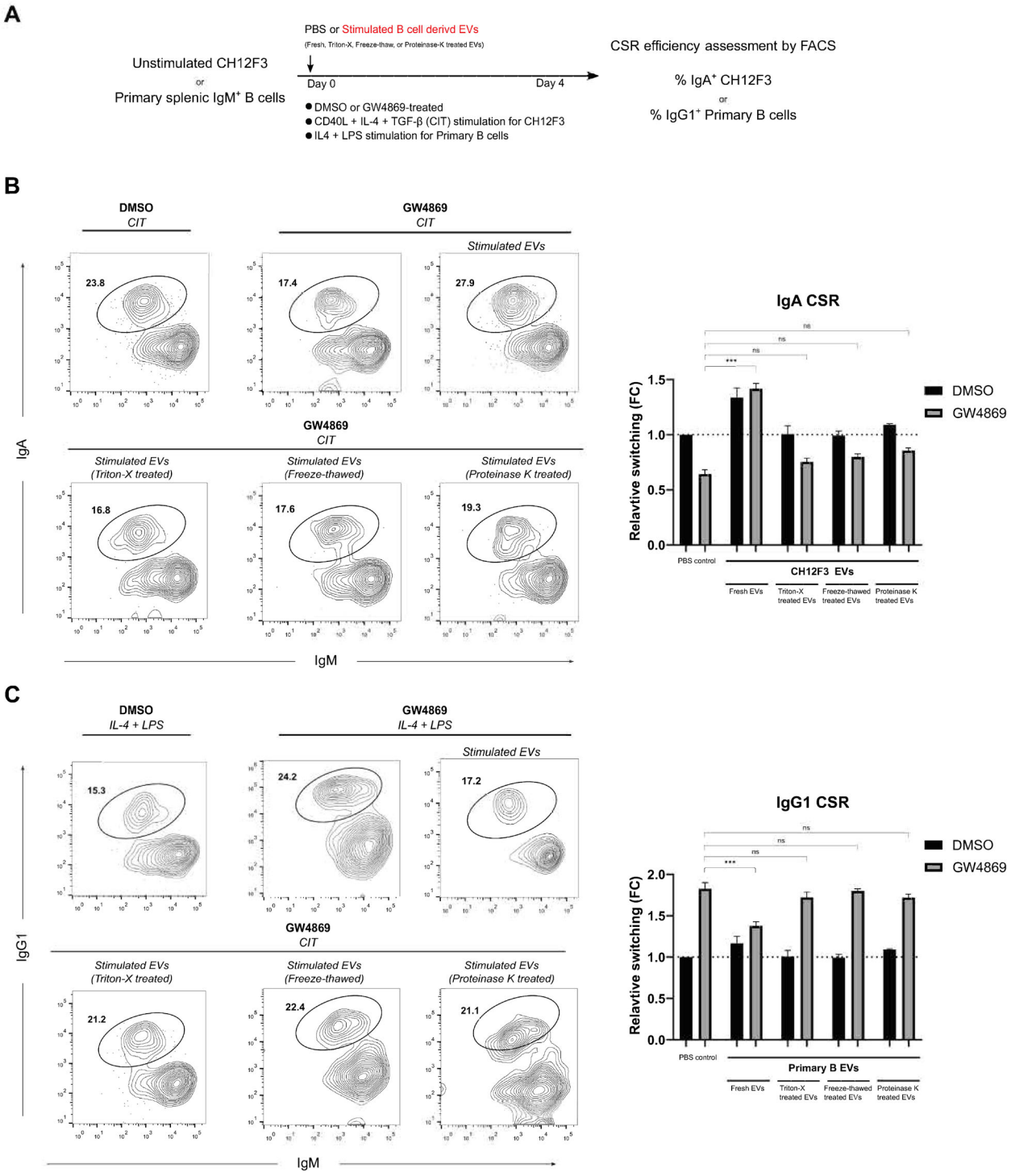

FIGURE 4 | CSR regulatory effects arise from different sources of EVs. (A) Schematic outline of functional phenotypic assay of EV-mediated CSR in CH12F3 (left) and primary B cells (right), 10 μM and 5 μM DMSO (negative control) and GW4869 was used to block EV production in CH12F3 and primary B cells respectively prior to cytokine activation. (B and C) Representative FACS plots and quantifications of CSR efficiency in either DMSO (mock), GW4869 (EV release inhibitor) with the addition of fresh EVs, proteinase-K treated EVs (surface antigens shaved), freeze-thawed, and Triton-X treated EVs (ruptured) in CH12F3 and primary B cells. Representative of three experiments, mean ±SD shown in columns by two-way ANOVA with Tukey's multiple comparison test (*$p < 0.05$; **$p < 0.01$; ***$p < 0.001$).

3.5 | EV ncRNA Cargo Are Responsible for CSR Regulation

EV ncRNAs cargo have been shown to modulate immune responses in vitro and in vivo (Yim et al. 2020). To identify the responsible EV ncRNAs in CSR modulation observed in Figure 1A,D, we focused on the significant DE miRNAs and DE lncRNAs in unswitched and switched parental cells and secreted EVs (Figure 5A, Supporting File 3). Expression of miR-5099, a miRNA enriched in germinal centre B cells compartment, was

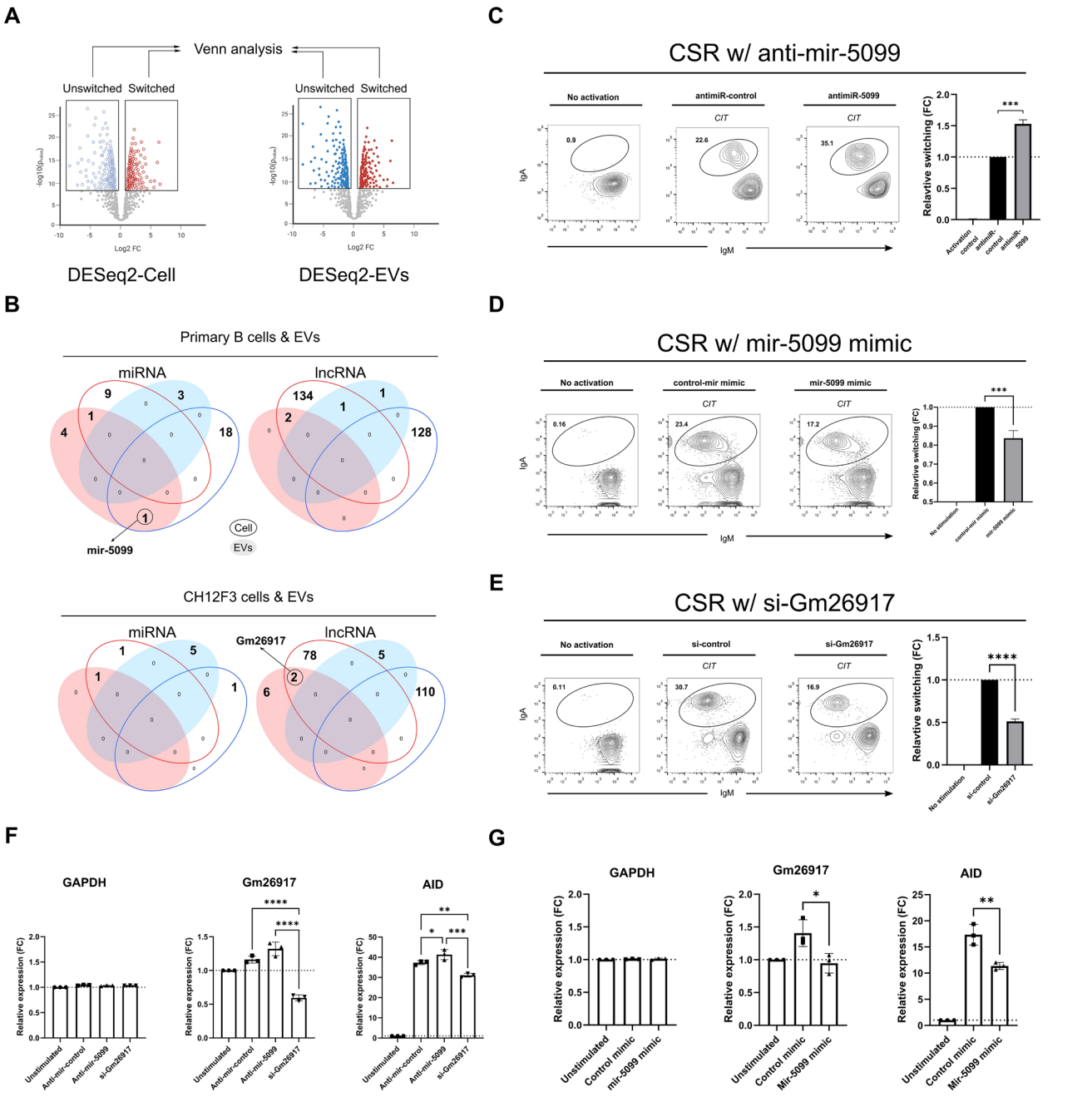

FIGURE 5 | EVs regulate CSR via the delivery of specific non-coding RNA. (A) Schematic outline of DESeq2 and Venn analysis of molecular cargo in EVs and paired cells during CSR. (B) Venn diagram analysis of differentially expressed ncRNA (Fold change ≥ 2, FDR < 0.05) in EVs and paired cells during CSR. (C-E) Representative FACS plots and quantifications of CSR efficiency in CH12F3 treated with anti-miR-5099 (C), miR-5099 mimic (D), and GapmeR Gm26917 (E) compared to respective negative controls. Representative of three experiments, mean ±SD shown in columns by one-way ANOVA with Tukey's multiple comparison test (*$p < 0.05$; **$p < 0.01$; ***$p < 0.001$). (F and G) Quantifications of relative expression of denoted genes in CH12F3 treated with anti-miR-5099 and GapmeR Gm26917 (F), and miR-5099 mimic compared to control (G), mean ±SD shown in columns by one-way ANOVA with Tukey's multiple comparison test (*$p < 0.05$; **$p < 0.01$; ***$p < 0.001$).

compared to known high expressers, AID and low expressers, Rag2 (Figure S10) (according to the Immunological Genome (ImmGen) consortium studies) (Heng et al. 2008). miR-5099 has no reported function in B cells nor other biological processes, was highly upregulated (Log_2 fold change = 3.653) in primary B EVs after stimulation. Interestingly, miR-5099 was downregulated (Log_2 fold change = −5.223) in the parental cells at the same time after stimulation (Figure 5B), suggesting primary B cells actively package miR-5099 into released EVs. To identify potential linkage to CSR-associated genes, we employed the ENCORI database to explore the interactive targets of miR-5099 (Table S1) (Li et al. 2014). Surprisingly, one of the two lncRNAs is upregulated in switched CH12F3 and secreted EVs, Gm26917 had the highest number of interactions and lowest minimum free energy of such RNA-RNA pairs. To probe the functional role of these two ncRNAs in CSR regulation, CH12F3 were treated with anti-miR-5099,

miR-5099 mimic and antisense LNA GapmeR for Gm26917 prior to CSR. Both anti-miR-5099 and GapmeR Gm26917 were labelled with FAM which enabled us to directly quantify the corresponding uptake in cells by FACS. miR-5099 mimic was co-transfected with GFP plasmid by nucleofection to confirm transfection efficiency (Figure S11). Strikingly, inhibition of miR-5099 leads to significant increase in both cell types compared to control, suggesting miR-5099 is a pan CSR suppressor in B cells (Figures 5C and S8). To confirm the CSR suppressing role of miR-5099, CH12F3 were transfected with miR-5099 mimic and subjected to CSR. Overexpression of miR-5099 led to drastic CSR reduction compared to control (Figure 5D), this further suggested miR-5099 is used by primary B cells to actively regulate CSR via EV-mediated signalling (Figure 6). Since Gm26917 is one of the most significant DE lncRNAs in CH12F3 EVs during CSR and is the top interactive target of the CSR suppressor miR-5099, we tested whether Gm26917 also involved in CSR regulation. Notably, the silencing of Gm26917 by antisense LNA oligonucleotides in CH12F3 has reduced CSR by 40%, suggesting the CSR-promoting role of Gm26917 (Figure 5E). Inhibition of mir-10b, one of the upregulated miRNAs in CH12F3 EVs post-CSR did not affect CSR efficiency, showing the specificity of identified ncRNAs (Figure S12). To confirm the interaction between miR-5099 and Gm26917 and associated CSR phenotypes, the expression of Gm26917 and AID was quantified in anti-miR-5099 treated, miR-5099 mimic and GapmeR Gm26917 treated CH12F3 during CSR by RT-qPCR (Figure 5F. Inhibition of miR-5099 reduced AID expression and increased Gm26917 expression, showing the CSR regulatory role of miR-5099 and the interaction between miR-5099 and Gm26917. In GapmeR Gm2617, the reduced Gm26917 expression confirmed the effective silencing of Gm26917. Reduction of AID in GapmeR Gm26917 treated CH12F3 suggested its CSR-promoting role. In contrast, overexpression of miR-5099 reduced Gm26917 expression and increased AID expression (Figure 5F,G), suggesting that Gm26917 could potentially be a suppressor of the CSR suppressor, miR-5099.

3.6 | EV miR-5099 Suppress CSR via Interaction With ROD1

To understand the downstream mechanism of CSR suppressor miR-5099, RNA-seq was performed with stimulated primary B cells treated with either anti-mir-control or anti-miR-5099. Interestingly, the transcript of the RNA binding protein, ROD1 (also known as PTBP3) was upregulated in anti-miR-5099 treated primary B cells compared to the control (Figure 6A). ROD1 has already been reported to interact with AID and serves as an essential guiding system for AID to the Ig loci during CSR in ex vivo studies (Chen et al. 2018). The other two members of this gene family PTBP1 and PTBP2 are also known to be essential for B cell maturation and development by controlling mRNA abundance and alternative splicing of vital cell cycle regulators (Monzón-Casanova et al. 2020; Monzón-Casanova et al. 2021, Sasanuma, Ozawa and Yoshida 2019). To confirm the interaction between miR-5099 and ROD1 at the transcription level, the expression of ROD1 was quantified in anti-miR-5099- and miR-5099 mimic-treated B cells after CSR. Upon treatment with anti-miR-5099, ROD1 expression was increased by 15% compared to control. Although in miR-5099 mimic-treated CH12F3, ROD1 expression was decreased by 25% compared to control. ROD1 expression was

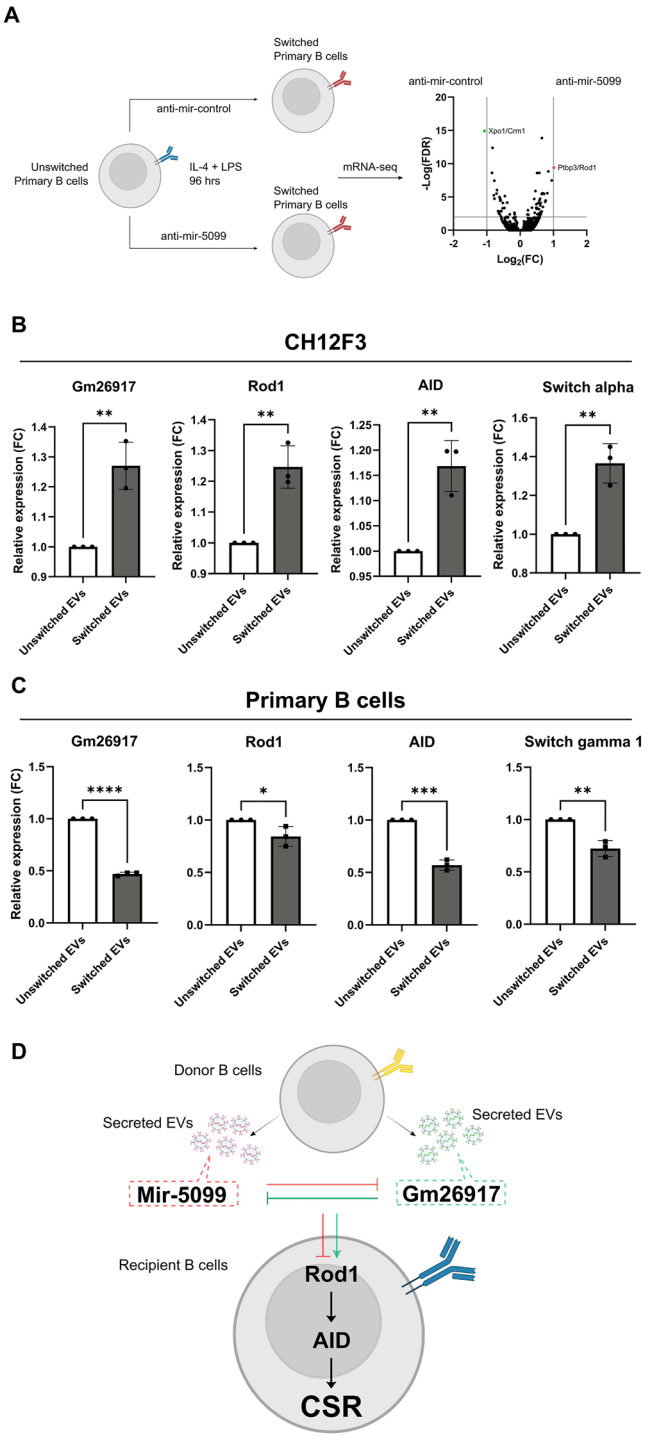

FIGURE 6 | B EV ncRNAs regulate CSR through PTBP3/Rod1 pathway. (A) Schematic outline of mRNA-seq of primary B cells treated with anti-miR-5099 and volcano plot showing differentially expressed downstream mRNAs in anti-miR-5099 treated cells compared to control. (B and C) Quantifications of relative expression of denoted genes in recipient CH12F3 (B) and primary B cells (C) in the presence of autologous EVs (unswitched and switched parental cells) 48 h post stimulation. On average 2×10^8 EV particles were used per condition. Mean ±SD shown in columns by one-way ANOVA with Tukey's multiple comparison test (*$p <$ 0.05; **$p < 0.01$; ***$p < 0.001$). (D) Proposed mechanism of B EV-mediated CSR regulation.

also decreased upon silencing of Gm26917, suggesting Gm26917 indirectly affect ROD1 expression possibly via interaction with miR-5099 (Figure S13). Next, we attempted to confirm that this novel CSR regulation is mediated by EV signalling, expression of Gm26917, ROD1, AID, switch alpha (CH12F3) and switch gamma 1 (primary B cells) were quantified in recipient CH12F3 and primary B cells in the presence of autologous EVs (either from unswitched and switched parental cells) 48 h post stimulation. As expected, Gm26917, ROD1, AID and switch alpha showed a significant increase in CH12F3 with the presence of autologous EVs from switched parental cells compared to unswitched control (Figure 6B). In contrast, expression of Gm26917, ROD1, AID and switch gamma 1 were reduced in primary B cells with the presence of autologous EVs from switched parental cells compared to unswitched control (Figure 6C). Overall, our findings have revealed a novel intercellular epigenomic signalling form of CSR regulation via EVs in physiological B cell maturation (Figure 6D).

4 | Discussion

CSR is a crucial process for diversification of antibodies effector functions in adaptive immunity. The two main study models, primary splenic B cells and CH12F3, representatives of healthy and oncogenic respectively, have a significant variance in CSR efficiency that has not been explained by endogenous proteomic, genomic, transcriptomic, or epigenetic studies. Indeed, understanding the molecular mechanism contributing to such variance would enhance our knowledge of CSR regulation and treating CSR defect-associated diseases. From the CM exchange assay in Figure 1, we revealed a novel EV-mediated intercellular epigenomic CSR regulatory network in physiological conditions independent of T-cell signalling. These findings contributed to our understanding of the significant variance in CSR efficiency between primary splenic B cells and CH12F3; and provide novel insights into how B cells with different backgrounds (i.e., healthy vs. cancerous) utilise EV signalling to tightly regulate their autologous activation equilibrium. Our findings hold a promising potential of developing into an early diagnostic and alternative therapeutic applications in B cell-associated autoimmune disorders and cancers.

B cell-associated EV studies in physiological conditions are still in a growing phase compared to those in other diseased models and the tools for studying EVs have evolved tremendously in recent years. Therefore, to gain more accurate knowledge of our studied EVs, we applied cutting-edge single-particle nanoflow-based technology combined with conventional imaging techniques to establish the biological background of B cell-derived EVs during physiological CSR. From our TEM analysis of CH12F3, we identified exosome-sized (within 40–150 nm) EVs being secreted in an encapsulated bag format by 12% of the 2D imaged cells in 100^{th} of an actual cell cross-section (70 nm). Considering the cells are 3D structured in reality, every cell is estimated to secrete 10 bags of EVs at any given time point, indicating the constitutive intercellular EV communication between CH12F3. Such form of particle release was also observed in viral infected T cells, colorectal cancer cells, cardiac telocytes and gastrointestinal stromal tumours (Muratori et al. 2009; Valcz et al. 2019; Fertig, Gherghiceanu, and Popescu 2014; Junquera et al. 2016), we are the first to report such mode of secretion of EVs under physiological condition from B cells, possibly to enhance protection and stability for the individual EVs in the extracellular space. Since the mode of EV biogenesis and secretion are not yet fully understood in B cells, our work displayed a clear visualisation of such processes and laid the foundation for future EV studies focusing on B cell EV biogenesis and secretion pathways.

Apart from morphological analysis, we attempted to determine the biological properties in B cell EVs during CSR using NanoFCM. Previous studies were mostly based on bulk EV analysis relying on common EV markers (i.e., CD9, CD63 and CD81), however, a recent mass spectrometric study has shown the common EV markers were not as representative as one would expect of the total EV population in multiple cancers derived EVs (Hoshino et al. 2020). With the aid of a single particle nanoflow analyser and silica sizing beads, we could determine the size of B cells EVs which is very comparable to the TEM data, as well as the estimation of EV secretion post activation that is in parallel to previous publications in a more robust and efficient manner (Muntasell, Berger, and Roche 2007; Saunderson et al. 2008). These findings could be further applied in other types of immune EV studies such as myeloid and lymphoid responses in research and clinical sectors.

One of the hallmarks of EVs is the expression of parental cell markers on their surface which allows EVs to be a novel immune response progression monitoring tool (Yim et al. 2020). With the aid of the nanoflow analyser, we determined the expression profile of EV enriched tetraspanins marker, B cell marker and CSR-associated markers on B cell EVs during CSR. Using HEK293A EVs as internal negative control, we can confirm the antibodies specificity from the low background signals observed. Conventional tetraspanin EV marker CD9 were expressed on 10% and 15% of total EVs released by stimulated CH12F3 and primary B cells respectively, suggesting studies relying on CD9 or other tetraspanins capture might not be conclusive in the total EV analysis. CSR associated markers, IgG1 (primary B cells) and IgA (CH12F3) were enriched in EVs derived from switched parental cells at 96 h post stimulation. Interestingly, IgM^+IgG1^+ and IgM^+IgA^+ EVs were detected in unswitched primary B cells and CH12F3 respectively at comparable levels (around 1%–2% of total EVs; $\sim 10^6$ EVs) to switched parental cells, indicating that in the absence of stimulation, B cells undergo stochastic CSR without expressing switched isotypes antibodies (IgG1 or IgA) on their surface but incorporated on released EVs by some means. These findings highlight the biological relevance of B cell derived EVs during physiological CSR and also the potential of being further utilised as a novel biomarker for early detection of B cell associated autoimmune diseases such as hyper IgM syndrome and cancers.

EV molecular cargo compositions have drawn much attention recently due to their ability to modulate intercellular signalling via targeted delivery of specific molecules such as RNA, DNA and proteins, particularly in ncRNA mediated gene regulation (Yim et al. 2020). In this study, ncRNA-seq was performed to understand the differential transcriptomic profile of B cell EVs during CSR as well as the variance of gene expression between parental cells and released EVs in both unswitched and switched states. From the complete DEG analysis and ImmGen database, we identified a novel CSR regulator, miR-5099, an

uncharacterised miRNA that suppresses CSR via EV-mediated intercellular signalling utilised by primary B cells, but not CH12F3. This data is indicating that healthy B cells suppress each other from hyperactivation via the delivery of EV-packaged miR-5099 between themselves, whilst the cancerous CH12F3 abolishes such machinery to increase hyperactivation. Gm26917, an uncharacterised lncRNA that was upregulated in CH12F3 EVs post stimulation, but not primary B cell EVs, it appeared to be a vital mediator for high CSR efficiency based on the Gm26917 silencing assay. Interestingly, Gm26917 is annotated as the top interacting target of miR-5099 from the ENCORI database, suggesting the high switching efficiency of CH12F3 possibly due to the high expression of Gm26917 and its suppression effect on miR-5099.

The mode of EV-mediated intercellular signalling could be very different depending on cell types, such as direct cargo transfer or receptor-mediated signalling (Cocozza et al. 2020). Understanding the mode of action in each study model is vital for future studies' direction. Interestingly, our data suggests EV-mediated CSR regulation in B cells are dependent on both EV surface receptors and intraluminal ncRNAs cargo to different extent as seen in the loss of CSR regulatory phenotype in both proteinase-K and triton-X treated EVs compared to fresh EVs. Since B cells are professional antigen-presenting cells within the immune system and producers of highly specific antibodies to neutralise pathogens or trigger professional effector cells (Sheppard et al. 2018), they are likely to benefit from these capacities to perform such strictly regulated signalling in autologous activation for CSR. Future studies and clinical applications could consider using B cells as primary EV producers, given the possibilities of shuttling specific cargo of interest and engineering the surface antigen repertoire, to provide an unprecedented level of targeted drug delivery.

Following the identification of miR-5099 and Gm26917, the mRNA-seq analysis of anti-miR-5099 treated primary B cells revealed the connection of miR-5099 to ROD1/PTBP3, an RNA-binding protein that has been shown as an essential factor for AID binding to the switch locus for CSR to occur (Chen et al. 2018). PTBP gene family has been reported in multiple literature in the context of B cell development and maintenance (Monzón-Casanova et al. 2020; Monzón-Casanova et al. 2021, Sasanuma, Ozawa, and Yoshida 2019). Furthermore, our findings bolstered the indispensable role of ROD1 in B cell CSR and divulged a novel intercellular epigenomic signalling network associated with ROD1 that ultimately leads to CSR regulation. In the translational diagnostics perspective, the level of EV miR-5099 circulating in the bloodstream can serve as a biomarker for early detection of B cell hyperactivation-associated autoimmune diseases and blood cancers. Therapeutically speaking, with the ability to specifically package and isolate miR-5099 enriched EVs from B cells, EV delivery of miR-5099 can ultimately be a form of drug treatment against hyperactivation of B cells associated with autoimmune diseases and blood cancers. It is worth noting that EV-mediated RNA transfer remains a topic of ongoing debate regarding the efficiency of EV cargo delivery (Albanese et al. 2021, Valadi et al. 2007). Although our data support a role for miR-5099 and Gm26917 in CSR regulation, we acknowledge that definitive proof of EV-mediated delivery remains technically challenging. Future studies employing approaches such as in situ RNA tracking and genetic manipulation of donor and acceptor cells will be essential to address this debate more conclusively.

Although our proposed novel EV-mediated CSR regulatory mechanism has provided a solid foundation and proof of concept for future studies in this direction, we believe there are far more unknown targets and alternative pathways underneath the full picture behind such EV-mediated epigenomic signalling in B cell CSR regulation but also other immune cells activation or suppression.

Author Contributions

Kevin Ho Wai Yim: conceptualization (supporting), data curation (lead), formal analysis (lead), investigation (supporting), methodology (equal), resources (supporting), software (equal), validation (equal), visualization (equal), writing–original draft (lead), writing–review and editing (supporting). **Alaa Al Hrout**: data curation (supporting), formal analysis (supporting), methodology (supporting), visualization (supporting), writing–review and editing (supporting). **Richard Chahwan**: conceptualization (lead), data curation (equal), formal analysis (supporting), funding acquisition (lead), investigation (lead), methodology (equal), project administration (lead), resources (lead), software (supporting), supervision (lead), validation (equal), visualization (supporting), writing–original draft (supporting), writing–review and editing (lead).

Acknowledgements

We thank the Exeter Sequencing facility particularly Paul O'Neil and Karen Moore for help and advice. Christian Hacker and UZH microscopy facility for TEM support and advice. Bogdan Mateescu for discussions. Profs Matthew Scharff and Christian Münz for critical reading of the manuscript. R.C. is supported by SNF (310030_212553; 320030E_215576, CRSK-3_190550; IZSEZ0_204655; IZSEZ0_218166), Novartis Foundation (22B140), Vontobel Stiftung (41309), UZH-STWF (F-41309-01-01) and the UZH-URPP (Translational Cancer Research). K.Y. is supported by a BioMedTech Entrepreneur Fellowship, BRIDGE-SNF (40B1-0_221565) and GRS-Innobooster (GRS-069/23). Funding for open access charge: SNSF-Chronoshub.

Conflict of Interest

The authors declare no conflicts of interest.

Data Availability Statement

Data are deposited in the GEO database with the accession number GSE242731.

References

Admyre, C., B. Bohle, S. M. Johansson, et al. 2007. "B Cell-Derived Exosomes Can Present Allergen Peptides and Activate Allergen-Specific T Cells to Proliferate and Produce TH2-Like Cytokines." *Journal of Allergy and Clinical Immunology* 120: 1418–1424.

Albanese, M., Y. F. A. Chen, C. Hüls, et al. 2021. "MicroRNAs Are Minor Constituents of Extracellular Vesicles That Are Rarely Delivered to Target Cells." *PLos Genetics* 17, no. 12: e1009951.

Bailey, T. L., J. Johnson, C. E. Grant, and W. S. Noble. 2015. "The MEME Suite." *Nucleic Acids Research* 43: W39–W49.

Bonilla, F. A., and H. C. Oettgen. 2010. "Adaptive Immunity." *Journal of Allergy and Clinical Immunology* 125, no. 2: S33–S40.

Chahwan, R., J. M. M. van Oers, E. Avdievich, et al. 2012. "The ATPase Activity of MLH1 Is Required to Orchestrate DNA Double-Strand Breaks

and End Processing During Class Switch Recombination." *Journal of Experimental Medicine* 209: 671–678.

Chen, J., Z. Cai, M. Bai, et al. 2018. "The RNA-Binding Protein ROD1/PTBP3 Cotranscriptionally Defines AID-Loading Sites to Mediate Antibody Class Switch in Mammalian Genomes." *Cell Research* 28, no. 10: 981–995.

Chettimada, S., D. R. Lorenz, V. Misra, et al. 2018. "Exosome Markers Associated With Immune Activation and Oxidative Stress in HIV Patients on Antiretroviral Therapy." *Scientific Reports*, 8, no. 1: 7227.

Cocozza, F., E. Grisard, L. Martin-Jaular, M. Mathieu, and C. Théry. 2020. "SnapShot: Extracellular Vesicles." *Cell* 182: 262–262.e1.

Essandoh, K., L. Yang, X. Wang, et al. 2015. "Blockade of Exosome Generation With GW4869 Dampens the Sepsis-Induced Inflammation and Cardiac Dysfunction." *Biochimica et Biophysica Acta Molecular Basis of Disease* 1852: 2362–2371.

Fan, Y., K. Siklenka, S. K. Arora, P. Ribeiro, S. Kimmins, and J. Xia. 2016. "miRNet—Dissecting miRNA-Target Interactions and Functional Associations Through Network-Based Visual Analysis." *Nucleic Acids Research* 44: W135–W141.

Fertig, E. T., M. Gherghiceanu, and L. M. Popescu. 2014. "Extracellular Vesicles Release by Cardiac Telocytes: Electron Microscopy and Electron Tomography." *Journal of Cellular and Molecular Medicine* 18: 1938–1943.

Garcia-Martin, R., G. Wang, B. B. Brandão, et al. 2022. "MicroRNA Sequence Codes for Small Extracellular Vesicle Release and Cellular Retention." *Nature* 601: 446–451.

Hale, J., K. Hughes, S. Hall, and R. Labens. 2021. "Effects of Production Method and Repeated Freeze Thaw Cycles on Cytokine Concentrations and Microbial Contamination in Equine Autologous Conditioned Serum." *Frontiers in Veterinary Science* 8: 759828.

Heng, T. S. P., M. W. Painter, K. Elpek, et al. 2008. "The Immunological Genome Project: Networks of Gene Expression in Immune Cells." *Nature Immunology* 9: 1091–1094.

Ho, K., W. Yim, S. Borgoni, and R. Chahwan. 2022. "Serum Extracellular Vesicles Profiling Is Associated With COVID-19 Progression and Immune Responses." *Journal of Extracellular Biology* 1: e37.

Hoshino, A., H. S. Kim, L. Bojmar, et al. 2020. "Extracellular Vesicle and Particle Biomarkers Define Multiple Human Cancers." *Cell* 182, no. 4: 1044–1061. e18.

Hu, H. Y., C. H. Yu, H. H. Zhang, et al. 2019. "Exosomal miR-1229 Derived From Colorectal Cancer Cells Promotes Angiogenesis by Targeting HIPK2." *International Journal of Biological Macromolecules* 132: 470–477.

Jhamnani, R. D., C. J. Nunes-Santos, J. Bergerson, and S. D. Rosenzweig. 2018. "Class-Switch Recombination (CSR)/Hyper-IgM (HIGM) Syndromes and Phosphoinositide 3-Kinase (PI3K) Defects." *Frontiers in Immunology* 9: 2172.

Ji, X., M. Wang, L. Li, et al. 2017. "The Impact of Repeated Freeze-Thaw Cycles on the Quality of Biomolecules in Four Different Tissues." *Biopreservation and Biobanking* 15: 475–483.

Junquera, C., T. Castiella, G. Muñoz, et al. 2016. "Biogenesis of a New Type of Extracellular Vesicles in Gastrointestinal Stromal Tumors: Ultrastructural Profiles of Spheresomes." *Histochemistry and Cell Biology* 146: 557–567.

Kosaka, N., H. Iguchi, Y. Yoshioka, F. Takeshita, Y. Matsuki, and T. Ochiya. 2010. "Secretory Mechanisms and Intercellular Transfer of microRNAs in Living Cells." *Journal of Biological Chemistry* 285, no. 23: 17442–17452.

Lee-Theilen, M., A. J. Matthews, D. Kelly, S. Zheng, and J. Chaudhuri. 2011. "CtIP Promotes Microhomology-Mediated Alternative End-Joining During Class Switch Recombination." *Nature Structural & Molecular Biology* 18: 75.

Li, J. H., S. Liu, H. Zhou, L. H. Qu, and J. H. Yang. 2014. "starBase v2.0: Decoding miRNA-ceRNA, miRNA-ncRNA and Protein–RNA Interaction Networks From Large-Scale CLIP-Seq Data." *Nucleic Acids Research* 42: D92–D97.

Liu, C., D. Chu, K. Kalantar-Zadeh, J. George, H. A. Young, and G. Liu. 2021. "Cytokines: From Clinical Significance to Quantification." *Advanced Science* 8, no. 15: e2004433.

Liu, J., E. Xiong, H. Zhu, et al. 2017. "Efficient Induction of Ig Gene Hypermutation in Ex Vivo-Activated Primary B Cells." *Journal of Immunology* 199: 3023–3030.

Monzón-Casanova, E., K. J. Bates, C. W. J. Smith, and M. Turner. 2021. "Essential Requirement for Polypyrimidine Tract Binding Proteins 1 and 3 in the Maturation and Maintenance of Mature B Cells in Mice." *European Journal of Immunology* 51: 2266–2273.

Monzón-Casanova, E., L. S. Matheson, K. Tabbada, K. Zarnack, C. W. Smith, and M. Turner. 2020. "Polypyrimidine Tract-Binding Proteins Are Essential for B Cell Development." *Elife* 9: e53557.

Morrish, R. B., M. Hermes, J. Metz, et al. 2019. "Single Cell Imaging of Nuclear Architecture Changes." *Frontiers in Cell and Developmental Biology* 7: 141.

Muntasell, A., A. C. Berger, and P. A. Roche. 2007. "T Cell-Induced Secretion of MHC Class II–Peptide Complexes on B Cell Exosomes." *European Molecular Biology Organization Journal* 26: 4263.

Muramatsu, M., K. Kinoshita, S. Fagarasan, S. Yamada, Y. Shinkai, and T. Honjo. 2000. "Class Switch Recombination and Hypermutation Require Activation-Induced Cytidine Deaminase (AID), a Potential RNA Editing Enzyme." *Cell* 102: 553–563.

Muratori, C., L. E. Cavallin, K. Krätzel, et al. 2009. "Massive Secretion by T Cells Is Caused by HIV Nef in Infected Cells and by Nef Transfer to Bystander Cells." *Cell Host & Microbe* 6: 218–230.

Nakamura, M., S. Kondo, M. Sugai, and M. Nazarea. 1996. "High Frequency Class Switching of an lgM + B Lymphoma Clone CH12F3 to lgA + Cells." *International Immunology* 8: 193–201.

Ramachandran, S., R. Chahwan, R. M. Nepal, et al. 2010. "The RNF8/RNF168 Ubiquitin Ligase Cascade Facilitates Class Switch Recombination." *Proceedings of the National Academy of Sciences* 107: 809–814.

Sasanuma, H., M. Ozawa, and N. Yoshida. 2019. "RNA-Binding Protein Ptbp1 Is Essential for BCR-mediated Antibody Production." *International Immunology* 31: 157–166.

Saunderson, S. C., P. C. Schuberth, A. C. Dunn, et al. 2008. "Induction of Exosome Release in Primary B Cells Stimulated via CD40 and the IL-4 Receptor." *Journal of Immunology* 180: 8146–8152.

Sheppard, E. C., R. B. Morrish, M. J. Dillon, R. Leyland, and R. Chahwan. 2018. "Epigenomic Modifications Mediating Antibody Maturation Frontiers Media S.A." *Frontiers in Immunology* 9: 355.

Simpson, S., J. Kaislasuo, S. Guller, and L. Pal. 2020. "Thermal Stability of Cytokines: A Review." *Cytokine* 125: 154829.

Thomas-Claudepierre, A. S., E. Schiavo, V. Heyer, et al. 2013. "The Cohesin Complex Regulates Immunoglobulin Class Switch Recombination." *Journal of Experimental Medicine* 210: 2495.

Trapnell, C., A. Roberts, L. Goff, et al. 2014. "Differential Gene and Transcript Expression Analysis of RNA-seq Experiments With TopHat and Cufflinks." *Nature Protocols* 7, no. 3: 562–578.

Valadi, H., K. Ekström, A. Bossios, M. Sjöstrand, J. J. Lee, and J. O. Lötvall. 2007. "Exosome-Mediated Transfer of mRNAs and microRNAs Is a Novel Mechanism of Genetic Exchange Between Cells." *Nature Cell Biology* 9: 654–659.

Valcz, G., E. I. Buzás, Á. Kittel, et al. 2019. "En Bloc Release of MVB-Like Small Extracellular Vesicle Clusters by Colorectal Carcinoma Cells." *Journal of Extracellular Vesicles* 8, no. 1: 1596668.

Vigorito, E., K. L. Perks, C. Abreu-Goodger, et al. 2007. "microRNA-155 Regulates the Generation of Immunoglobulin Class-Switched Plasma Cells." *Immunity* 27: 847.

Wang, S., K. Lee, S. Gray, et al. 2022. "Role of EXO1 Nuclease Activity in Genome Maintenance, the Immune Response and Tumor Suppression in Exo1D173A Mice." *Nucleic Acids Research* 50: 8093–8106.

Wang, Y., H. Zheng, J. Chen, et al. 2015. "The Impact of Different Preservation Conditions and Freezing-Thawing Cycles on Quality of RNA, DNA, and Proteins in Cancer Tissue." *Biopreserv Biobank* 13: 335–347.

Xu, Z., H. Zan, E. J. Pone, T. Mai, and P. Casali. 2012. "Immunoglobulin Class Switch DNA Recombination: Induction, Targeting and Beyond." *Nature Reviews Immunology* 12: 517.

Yim, K. H. W., A. Hrout Al, S. Borgoni, and R. Chahwan. 2020. "Extracellular Vesicles Orchestrate Immune and Tumor Interaction Networks." *Cancers (Basel)* 12: 1–23.

Yim, K. H. W., O. Krzyzaniak, A. Al Hrout, B. Peacock, and R. Chahwan. 2023. "Assessing Extracellular Vesicles in Human Biofluids Using Flow-Based Analyzers." *Advanced Healthcare Materials* 12: 32.

Zhang, Z., Y. Zhang, P. Evans, A. Chinwalla, and D. Taylor. 2017. "RNA-seq 2G: Online Analysis of Differential Gene Expression With Comprehensive Options of Statistical Methods." *bioRxiv* 122747. https://doi.org/10.1101/122747.

Supporting Information

Additional supporting information can be found online in the Supporting Information section.